Imperial College London

Use Deep Learning Networks and Digitized Herbarium Specimens to Study Leaf Evolution Patterns

Peter Zeng

August 2022

A thesis submitted for the partial fulfillment of the requirements for the degree of Master of Research at Imperial College London

Formatted in the journal style of the *Evolutionary Biology*

Submitted for the MRes in Computational Methods in Evolution and Ecology Research Project

Declaration

I here declare that this thesis, "Use Deep Learning Networks and Digitized Herbarium Specimens to Study Leaf Evolution Patterns" is my work, with the guidance from my supervisors Dr. Will Pearse, Dr. Gemma Bramley and Dr. Alexander Zuntini. All data used in this project has proper citations. The phylogeny (the GBMB tree) was built by Smith & Brown and available online (Smith & Brown (2018)). The images of herbarium specimens were collected by Royal Botanic Garden, Kew and downloaded by me through API search on GBIF website, and I filtered the masks generated from these images to select the masks that are suitable for analysis. The architecture of networks used in this project are designed by Facebook AI Research teams on detectron2 platform and the pre-train model is the model I downloaded from detectron2 model zoo (Kirillov *et al*., (2020); He *et al*., (2017)). The network structure figure is created with BioRender.com. The main packages I used for EFA, PCA and comparing model fitting are Momocs (Bonhomme *et al*, (2014)) and mvMORPH (Clavel *et al*. (2015)). My supervisors guided my research direction, suggested research methodology and result explanation and provided feedback on my thesis draft. I herewith certify that all material in this dissertation which is not my own work has been properly acknowledged.

Name of Student: Peter Zeng
Supervisors: Dr. Will Pearse, Dr. Gemma Bramley, Dr. Alexander Zuntini

Date: 24/08/2022
Word Count: 5272

Contents

Abstract

Leaves are essential organs of plants, and there are many studies on their functional trait evolution. In particular, the study of morphological traits of leaves provides important physiology and ecology evidence, and studying morphological traits evolution patterns provide evidence of plants' adaptation to environmental conditions and their interspecific relationships within communities and ecosystem. However, extracting morphological traits from leaves is hard, as it is very time-consuming and difficult to repeat the measurement of samples. Fortunately, with the development of computer vision and object segmentation methods, it is now possible to efficiently extract leaf segments from digitized herbarium specimens and automatically collect continuous morphometric traits to study leaf evolution. In this study, I built a pipeline that helped me efficiently analyze the evolutionary patterns from raw digitized herbarium specimens, which shows a new possible way to study leaf evolution.

Keywords: Leaf Evolution Patterns, Herbarium Specimens, Object Segmentation, Machine Learning, Trait Measurements, Phylogenetic Comparative Methods, Model Comparison, Traits Correlations

1 Introduction

Leaves, as the organs of plant that specialize in photosynthesis, are important to the growth and survival of plants. Plants need to trade-off between gain (energy and carbon) and cost (water and nutrients) of leaves (Poorter L., Bongers F., (2006)). Therefore, plants have different leaf investment strategies that are based on leaf functional traits, such as the morphological, biochemical, and physiological traits (Kröber *et al*., (2015); Adler *et al*., (2014); Gupta *et al*., (2020)). The functional traits of leaves evolve through time and cause huge variation among species, representing both plants' adaptation to environmental conditions and their interspecific relationships within communities and ecosystems (Reich *et al*., (1999); Reich *et al*., (1997); Lavorel & Garnier, (2002), Bruelheide *et al.*, (2018)). In this case, modeling the trait evolution helps understand the evolution force in traits variation and the correlation among multiple functional traits (*Reich et al*., (2003); Caetano D. S. & Harmon L. J., (2017)). By using phylogenetic comparative method (PCM) to fit different evolutionary models to one molecular-based phylogeny and trait measurements, it is possible to draw inferences and raise different hypotheses about tempo and mode in evolution, which reflects the evolution rate and how evolution rate changes through time. (Dornbusch *et al*., (2011); Figueirido *et al*., (2010); *Blomberg et al*., (2002); Cooper & Purvis (2010); Slater *et al*., (2012); Hunt, G., (2012)). Also, as traits might evolve in a correlated manner, comparing the strength of traits' evolutionary covariance to the variances on single traits can be important for studying correlated selection of plants (Cornwell *et al*., (2017); Caetano D. S. & Harmon L. J., (2017)).

However, there are limitations on collecting traits data when studying the evolution of functional traits. To perform reliable evolutionary studies, large-scale functional trait datasets are required. Manually measuring functional traits from samples can be highly time-consuming when the phylogeny is large. This causes many studies of traits evolution to focus on a limited number of species, which lose the chance to have a broader exploration (Smith S. A. & Brown J. W., (2018)). Beyond that, for many datasets, the measured samples were not preserved as specimens, which lost the opportunity to extract additional traits and repeat the measurements of traits (Weeks *et al*., (2022)). In this case, one potential solution is to extract traits from the digitized herbarium specimens preserved by the natural history museum or botanic garden (Hussein *et al*., (2021)). Many herbarium specimens have been collected and preserved, and their images are usually included in their digitized versions that are preserved online. From these images, potential morphological traits like leaf size and shape can be collected from the leaf segments in these specimens (Triki *et al*., (2021)). This can be done by measuring morphological metrics of leaf segments, such as leaf length, width, circularity, and shape descriptors, which can be considered morphological traits as well. These morphological metrics of leaves are preserved well when plants are made into two-dimensional herbarium specimens (Jones *et al*., (2009)). Since it is possible to collect morphological traits from metrics of leaf segments, if there is a method that can help researchers to efficiently extract leaf segments from enormous digitized herbarium specimens in a simple way, it can greatly help studying the evolution patterns of plants, which also benefits other studies of plants, such as the physiological, plant development and ecological study (Lusk C. H., (2002); Shi *et al*., (2019); Piazza *et al*., (2005)).

Previous studies to extract leaf segments focus on traditional statistical image process methods. These methods, such as thresholding (Easlon & Bloom, (2014); Katabuchi M, (2015)) and watershed methods (Rahman *et al*., 2013), are mainly based on finding the edges of the color change of pixels, representing the edges between leaves and background. However, when studying herbarium specimens, the image of the specimen always contains other objects that are not a part of the plant, such as color charts, scale rulers, and labels of plants. Though these objects provide additional information, they affect the performance of leaf extraction, as these methods cannot classify the segmented objects, and hard to extract only the leaf segments from specimens. Fortunately, the growth in computer vision field provides new methods in object classification, detection and segmentation (He *et al*., (2016); He *et al*., (2017)) based on deep learning networks. Previous studies have successfully used deep learning networks to extract target objects from the specimen image, showing the potential for a similar application in leaf extraction (Weeks *et al*., (2022); Liu *et al*., (2019), Triki *et al*., (2021)). In this case, after training an object segmentation network with a relatively small training dataset of leaves, the network can automatically extract leaf segments from the digitized herbarium specimen and ignore noise and irrelevant objects in the background. These leaf segments can then be used to collect morphological traits and thus model the evolutionary pattern of leaves (Adams & Otárola-Castillo, (2013)).

The focus of this project is to study leaf evolution patterns by using deep learning networks and digitized herbarium specimen. To do that, I built a pipeline that help me analyzing leaf evolutionary patterns from raw digitized herbarium specimens. Four steps are involved in this pipeline:

1. I downloaded images of herbarium specimens based on the taxa of a large seed plant phylogeny. Each taxon represents one seed plant species.
2. I trained a deep learning network to extract every leaf in the image as a mask.
3. I collected and evaluated morphological traits from leaf segments.
4. With these morphological traits and the phylogeny, I compared the fit of different evolutionary models by using phylogenetic comparative method (PCM).

From the result of model fitting and comparison, I drew inferences about tempo and mode in the evolution of leaf morphological traits and the correlation between traits.

2 Methods

2.1 Data Acquisition and Preparation

2.1.1 Downloading the Phylogenetic Tree

PCM requires traits to be compared across a phylogeny. A large phylogeny can help shed light on evolutionary patterns and serve as tools that facilitate comparative study (Smith S. A. & Brown J. W., (2018)). The phylogeny is the GBMB phylogeny which has 79,874 taxa of seed plants, each taxa represent one species. The phylogeny is built based on genetic data from GenBank with phylogenetic data from the Open Tree of Life project (Smith S. A. & Brown J. W., (2018)).

2.1.2 Downloading Herbarium Specimen Images

By searching the scientific name of each taxon in the GBMB phylogeny with API searching, I downloaded the herbarium specimen image collected by Royal Botanic Garden, Kew, from the GBIF website (Global Biodiversity Information Facility). I downloaded one image of each specimen, and I downloaded 37,245 digitized herbarium specimens that were collected by Kew Garden and uploaded to the GBIF website. An example of herbarium specimen image is shown in Fig. 1(a).

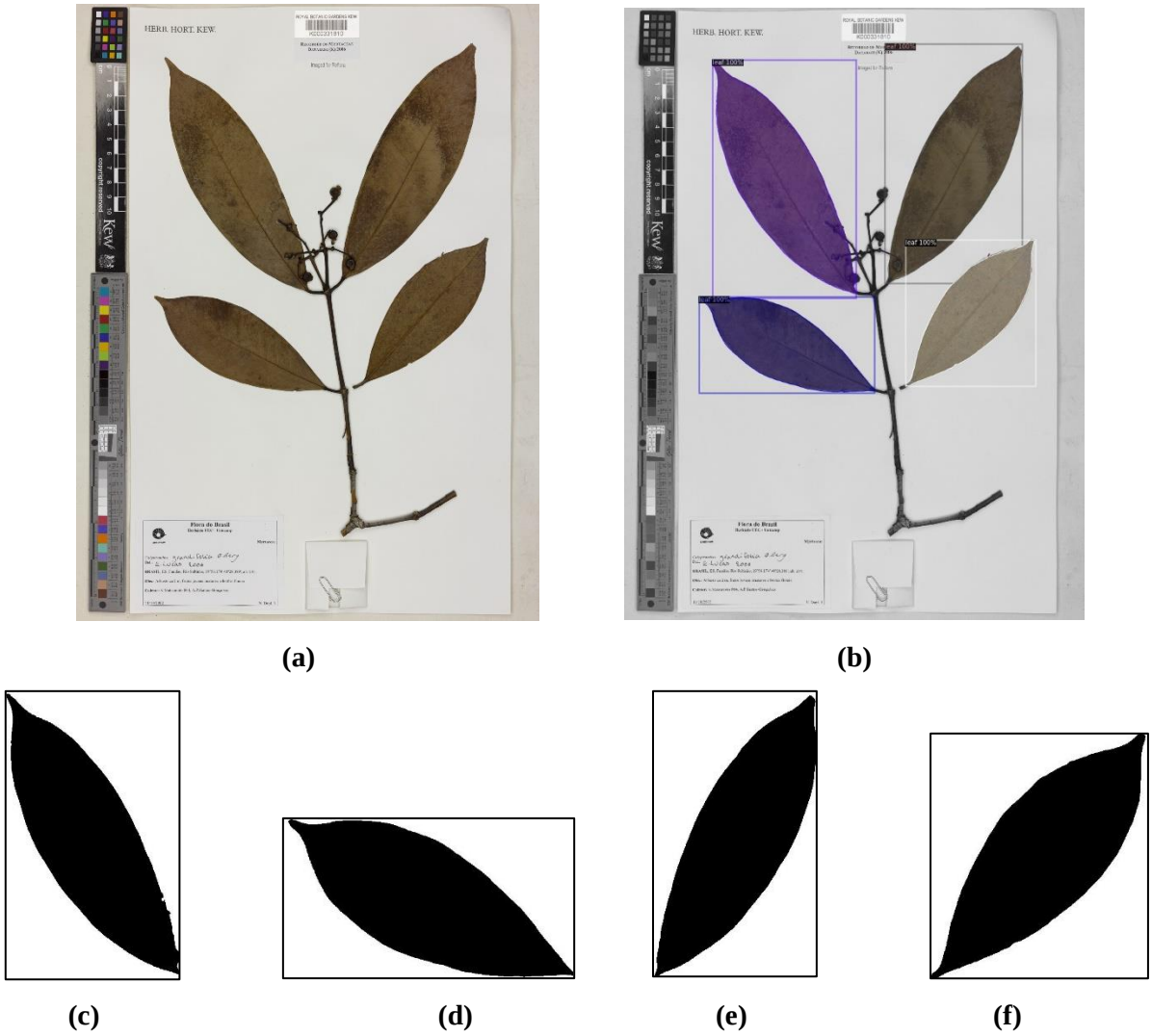

Fig. 1 An example of (a) the herbarium specimen image (b) masks and their positions on the specimen image (c) – (f) masks of leaf segments and their bounding boxes. Masks are the colorful region on the specimen image in (b) and the black regions in (c) – (f). Each mask has a bounding box that bound the masks. The percentage shown in each bounding boxes in (b) are the confidence level of the mask, which shows how confident the network classifies each object as a leaf. From this figure, we can see how masks cover the leaf segment in the herbarium specimen.

2.2 Deep Learning Network

2.2.1 Methods of object segmentation

The goal of using deep learning networks is to efficiently extract leaf segments as masks from the image of herbarium specimens and ignore the noisy background and irrelevant objects (Fig. 1(b)). Masks describe shapes of objects with true and false values in pixels, as the pixels with true value (represent with black color in a mask image) are parts of the object, whereas the pixels with false value (represent with white color in a mask image) represent the background (Fig. 1(c)-(f)). Initially, I used a classic Mask R-CNN (Region-Based Convolutional Neural Network) to perform object segmentation, which aims to extract and classify target

objects from the background (He *et al*., (2017)). However, since Mask R-CNN considers the input image as a regular grid of pixels with low resolution, it will naturally oversample the smooth interior areas while undersampling object boundaries (Kirillov *et al*., (2020)), generating a blurred outline, which is not ideal for further morphological analysis. More details and explanations about Mask R-CNN structure can be found in Supplement SI 1.

In this case, instead of using classic Mask R-CNN, I constructed a PointRend network based on the Mask R-CNN (Kirillov *et al*., 2020). PointRend is a module that improves the performance of Mask R-CNN or other object detection network, as the resultant masks produced by PointRend Mask R-CNN covers more details than classic Mask R-CNN mask (Kirillov *et al*., 2020). Comparison between masks generated by two networks is shown in Fig. 2.

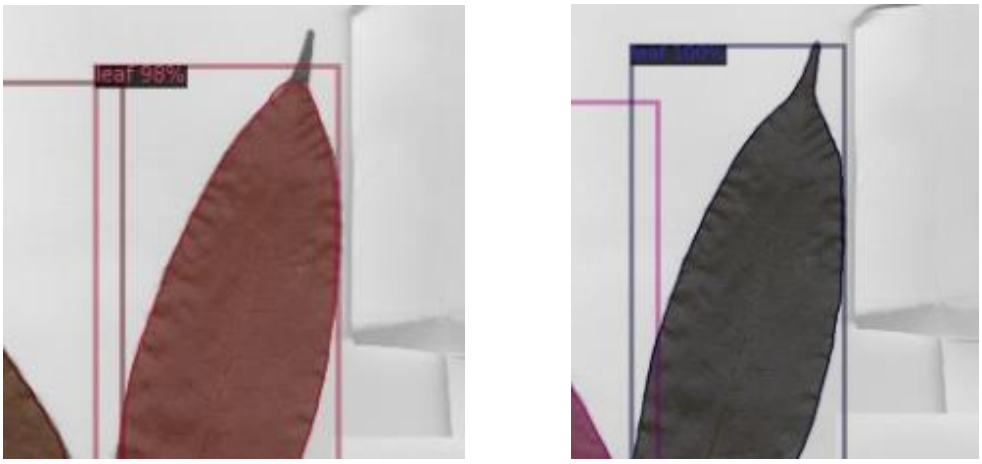

(a) **(b)**

Fig. 2. Comparison between (a) mask generated by Mask R-CNN and (b) mask generated by PointRend Mask R-CNN. This shows how Mask R-CNN and PointRend differ in their identification and extraction of leaves within images. As we can see, both networks are able to detect and segment leaves in digitized herbarium specimens. However, the mask from classic Mask R-CNN is not able to cover the tip of leaves into masks. PointRend Mask R-CNN successfully covers the leaf with masks, which provides a finer mask

The network's head and the network's backbone are the two main components that construct the network. Compared to the classic Mask R-CNN, the PointRend Mask R-CNN uses a PointRend head and the same Mask R-CNN backbone (Kirillov et al. 2020). I use ResNet-50 FPN as the backbone of the network, which is consisted of a residual network (ResNet) with 50 layers of neurons and a feature pyramid network (FPN) that helps extract features of the Regions of Interest (RoI), which are the regions that may contain target objects, from different levels of the feature map pyramid according to their scale (He *et al*., (2016); Lin *et al*., (2017)). A PointRend head module is then added to the backbone, which generates a coarse prediction at the beginning with a low-resolution feature map and re-predicts the points that are ambiguous in labeling with higher resolution feature maps around these points (Kirillov *et al*., 2020). This re-prediction of points will

repeat several times, and the resolution of the feature map gets higher each time, as it helps covers more detail and generates finer masks (Kirillov *et al*., 2020). An overview of PointRend Mask R-CNN architecture is shown in Fig. 3.

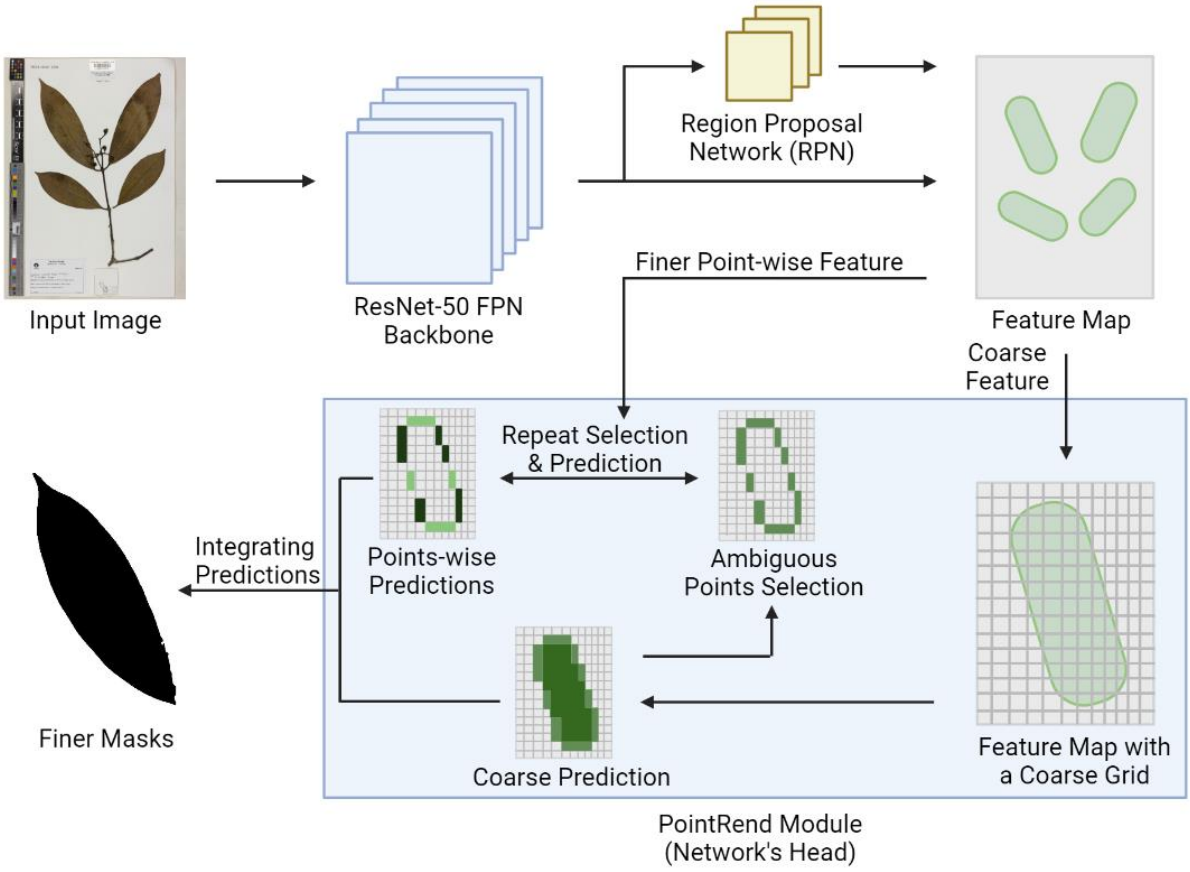

Fig. 3 An overview of the PointRend Mask R-CNN architecture. The depth of green color of pixels in PointRend Module visualize the confidence level of the classification, which shows how confident the network label the pixel as a part of a leaf segment. More details about PointRend module structure can be found in Supplement SI 2.

2.2.2 Annotation and Training PointRend Mask R-CNN

I manually annotated parts of digitized specimens to provide training and testing datasets to fine-tune the pre-trained model, as it is easier to train a pre-train model than to train a raw model directly (Pan *et al*., 2009). I annotated 100 herbarium specimens for training and 20 specimens for testing manually by using VGG Image Annotator (VIA), which is a manual annotation software. To annotate the outline of leaf segments, I use a polygon that follows the edge of the leaf segment in a Cartesian pixel coordinate system.

I fine-tuned a pre-trained ResNet-50 FPN model with my training datasets. The model has been trained on the Common Object in Context (COCO) dataset with the 3x schedule, which is about ~37 COCO epochs. Each epoch represents one complete pass of the COCO dataset through the algorithm. The learning rate I used is 0.00010. I trained the network with nine cycles, which have 6000 epochs in each cycle, as my training dataset is much smaller than the COCO datasets. For generating the output, I used a confidence level of 0.9, which means only masks with a confidence level of labeling the class higher than 0.9 will be selected.

2.3 Morphological Trait Extraction

2.3.1 Leaf Outline Extraction

Before extracting traits from masks, the outlines of the masks need to be extracted as polygons on the coordinate system first. The function of outline extraction is provided by Momocs, which is a complete toolkit for morphometrics analysis in R (Bonhomme *et al*, (2014)).

2.3.2 Evaluating Leaf Area from Leaf Masks

Leaf area is evaluated to represent leaf size (Schrader *et al*., (2021)). For each mask, the number of pixels covered by the mask has been counted, which represents the area of each mask. Before model fitting and further analysis, the values of leaf area are normalized to reduce redundancy and complexity by min-max normalization. The min-max normalization is performed by centering the values of the leaf area and then dividing the value by the max and min value of the leaf area.

2.3.3 Describing Leaf Shape with Elliptic Fourier Analysis

I use elliptic Fourier analysis (EFA) to describe the leaf shape (Kuhl & Giardina, (1982)). To perform EFA, the outline of the leaf mask is described with several trigonometric functions in a Cartesian coordinates system. From these trigonometric functions, harmonic coefficients can be calculated. For each harmonic, four harmonic coefficients (A_n, B_n, C_n, D_n) can be described (Caple *et al*., (2017)). With these harmonic coefficients for each harmonic, it is possible to express a shape that describes the outline of a mask, as shown in Fig. 4. Details about EFA algorithm can be found in Supplementary SI 3.

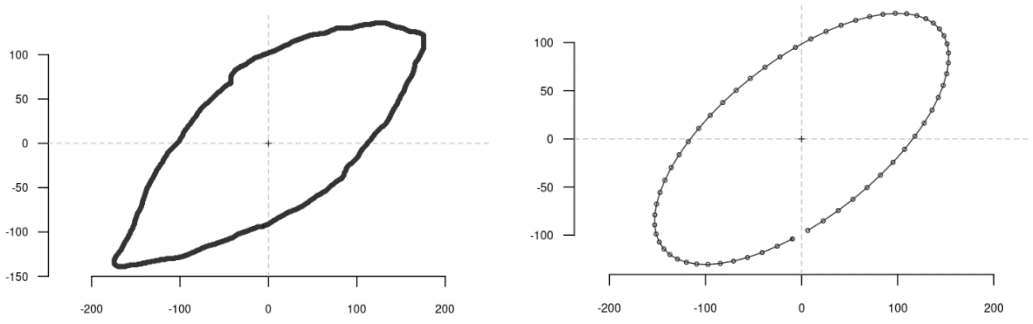

(a) (b)

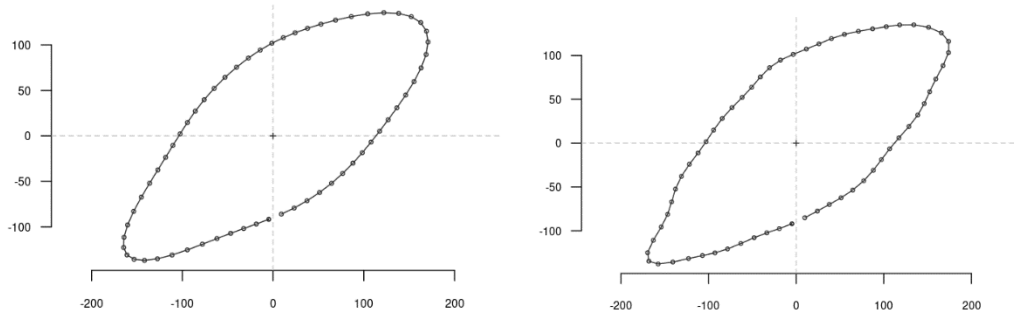

(c) (d)

Fig. 4 An example of leaf mask outline and its EFA expression. (a) the original mask outline describes by points (b) elliptic Fourier shape with 1 harmonic (c) elliptic Fourier shape with 5 harmonic (b) elliptic Fourier shape with 12 harmonics. As we can see from the shapes expressed by harmonic coefficients, when the number of harmonics gets higher, the resultant shapes become more precise and closer to the original outline.

To describe the outline of the leaf precisely, the frequency of the harmonic must be high enough. This will generate a high number of harmonic coefficients, which are hard to analyze directly by PCM. Therefore, it is necessary to perform dimension reduction on these coefficients using principal component analysis (PCA), which projects each harmonic coefficient onto a few principal components (PC) and preserves the variation of these coefficients (Caple *et al*., (2017)). These PCs can be considered as continuous morphometric traits to study the evolutionary patterns of leaves, especially the first few PCs, since small changes in these PCs will significantly influence the expression of leaf shape. Therefore, studying the similarities and differences of these PCs can also reflect phylogenetic relationships and evolutionary patterns (Harmon *et al*., (2010); Klingenberg *et al*., (2013); Schmittbuhl *et al*., (2002)).

The PCA functions used in this project are provided by Momocs, and they are originally based on the ade4 package (Bonhomme *et al*., (2014)). I described the leaf shapes with 12 harmonics, which generates 48 harmonic coefficients for each leaf mask. PCA is performed on harmonic coefficients to extract PCs, and the first three PCs are used in PCM to study the evolution of the leaf shape and compare the correlation between PCs.

2.3.4 Filtering the Masks

Although PointRend Mask R-CNN generates finer masks than classic Mask R-CNN, it is still necessary to filter the output mask. The leaves of herbarium specimens are usually damaged and stuck together, and it significantly affects the result of morphological analysis if masks of these unqualified leaves are used. In this case, I used the random forest (RF) method to filter the masks, which is a supervised machine learning

algorithm that is widely used in classification and regression problems (Breiman L, (2001); Speiser *et al*., (2019)).

In this project, RF method uses morphological metrics to classify each mask into qualified masks or unqualified masks, and qualified masks are passed for further analysis. I extract eight morphological metrics for each mask, which are (1) area (2) perimeter (3) length (4) width (5) circularity (measurement of the roundness) (6) elongation (ratio of the width/length) (7) calipers length (longest distance between two points of the leaf shape) (8) convex hull area.

For training the RF model, I manually labeled 1,904 masks for providing training and validating the dataset, of which 485 masks are labeled as qualified masks.

After filtering the mask, I also perform filtering based on specimens. The specimens with only 1 and 2 masks left after filtering by RF methods are also filtered out, as these specimens do not have enough masks to represent the average size and shape of their leaves. I also filtered out the specimens that have a relatively high variance (the higher outliers) on each mask's PCs, which implies there is a high possibility that the fragments of leaves are involved. After these specimen filtering steps, I randomly choose one mask for each specimen. These masks represent their own species and are used for the PCM analysis.

2.4 Comparing the Fitting of Evolution Models

Comparing the fitting of evolution models leads to the inference of tempo and mode of evolutionary patterns. I compared the fitting of the Brownian Motion (BM) model and the Ornstein Uhlenbeck (OU) model, which are the most widely used evolutionary models in PCM study (Revell *et al*., (2008)). BM model considers the evolution mode of traits to be random walks, and the average rate of evolution should be approximately zero in the long run (Cornwell *et al*., (2017); Hunt G., (2012)). The model is based on the equation (1):

$$dX(t) = \sigma dB(t) \qquad (1)$$

Here, $dX(t)$ represents the change in trait. $dB(t)$ represents the branch length, which is the evolutionary time between two nodes on a phylogeny. σ is the rate of evolution of Brownian motion.

Based on the BM model, the Ornstein Uhlenbeck (OU) model adds a pulling force toward one or several optimums due to the stabilizing selection or other reasons (Cooper *et al*., 2016). The model is based on equation (2):

$$dX(t) = \alpha[\theta - X(t)]dt + \sigma dB(t) \qquad (2)$$

$\alpha[\Theta - X(t)]dt$ represents the pulling force towards optimums. If α is smaller, the pull force is smaller. Θ represent the optimum state of trait, and X(t) represent the current state of trait. $\Theta - X(t)$ represent the difference of traits towards optimums, and if the difference is larger, this makes pulling force become larger. $\sigma dB(t)$ represent the random walk, which is the same as the one in BM model.

I used the mvMORPH package for fitting the evolutionary models to the phylogeny and traits, which are the first three PCs of harmonic coefficients and area of leaves (Clavel *et al*., (2015)). For the result of fitting, the evolution rate matrices were calculated. Evolution rate matrices are variance-covariance matrices that describe rates of trait evolution in the diagonals and the evolutionary covariance among traits in the off-diagonals, which reflect the evolutionary correlation among multiple traits (Caetano D. S. & Harmon L. J., (2017)). The correlation between traits can be calculated by equation (3).

$$\rho_{xy} = \frac{Cov(x,y)}{\sqrt{Var(x)} * \sqrt{Var(y)}} \qquad (3)$$

ρ_{xy} represents the correlation between two traits. $Cov(x,y)$ represent the covariance of x and y. $Var(x)$ and $Var(y)$ represent the variance of each trait.

The resultant Akaike Information Criterions (AICs) of model fitting are calculated based on the maximum log-likelihood of the models and the numbers of parameters, which are used to compare different evolution models' fitting.

3 Results

3.1 PointRend Mask R-CNN Masks Extraction

Loss is a metric used to assess how a deep learning model fits the training data. After training, the loss of the network training becomes stable. Each loss has the same weight when calculating the total loss. The total loss of the network is 0.462, and the loss of mask point, which is a unique loss of PointRend that measures the loss of point-wise labeling, is 0.2269 and counts for about half of the total loss. The loss reaches a relatively low level and means that the deep learning model fits the training data well.

The Mask R-CNN based PointRend Network processed 41,903 species in total. Each species provides one digitized herbarium specimen image for mask extraction. In sum, the network detected and extracted leaf segments in 19,019 specimens, which provides me with 309,197 masks that have a confidence level higher

than 0.9. Besides masks, I also generated the images of each specimen together with the corresponding masks for each mask.

3.2 Filtering Masks

Several steps of mask filtering were performed to select masks with qualified shapes. For computational convenience, I randomly chose 25% of the masks, of which 77,299 masks from 4,505 specimens remained. After filtering by the RF model, 14,174 masks remained, which are from 3,333 specimens. Then, I filtered out the specimen with few masks, of which 1,736 specimens remained. Finally, after filtering out the specimens that have relatively high variances within each of the first 3 PCs, I got 1,019 specimens, which are the specimens I used for further analysis. For each specimen, one mask is randomly chosen to represent the overall specimen.

3.3 Morphological Traits Extractions

After the outline had been extracted as polygon points, EFA was performed on these outline points. Based on harmonic coefficients, PCA was performed to extract the principal components, and I visualized the morphological variations across these PCs in a morphospace (Fig. 5).

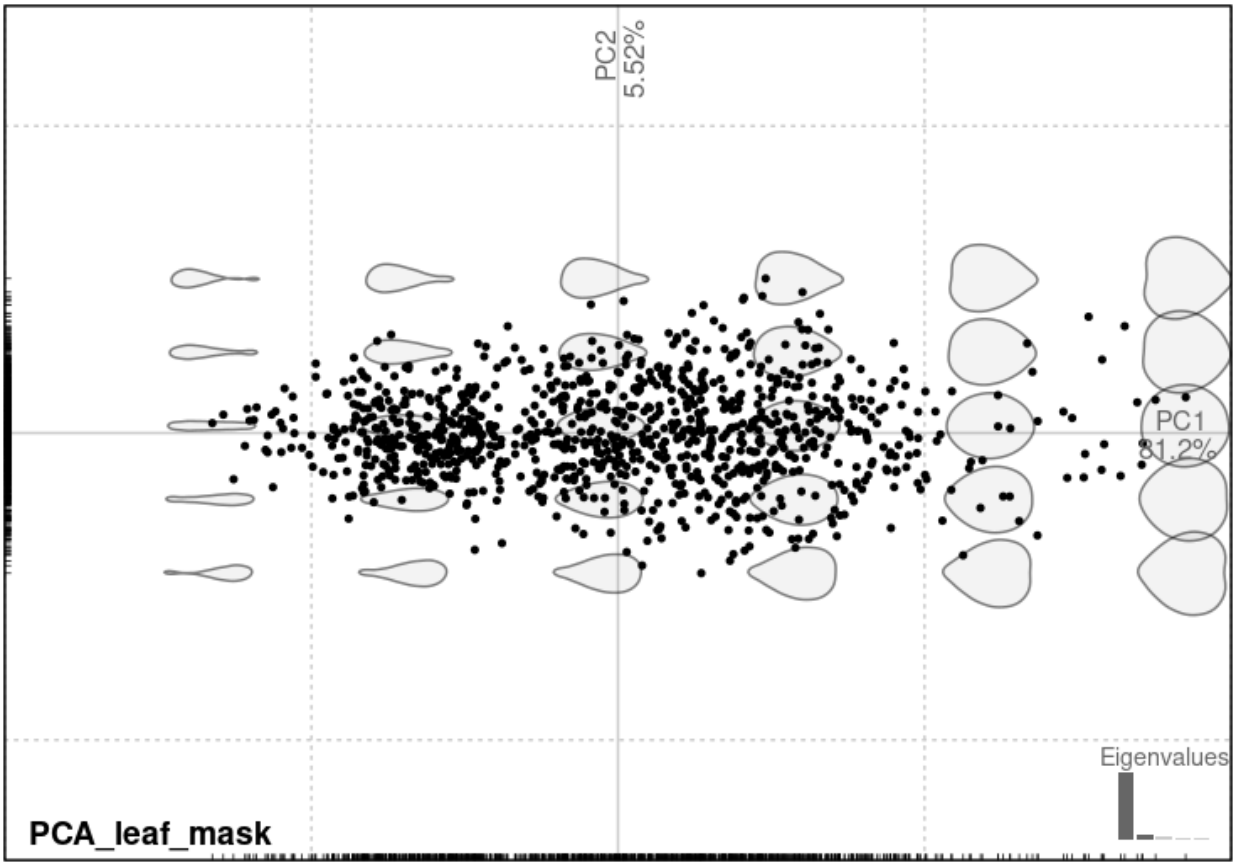

Fig. 5 2D morphospace graph of the leaf shape with PC1 and PC2. Each point represents one specimen. The leaf shapes shown in the morphospace graph are theoretical shapes based on the harmonic coefficients. If the

points are close to one theoretical shape, this means that the masks of specimens are similar to that shape. The percentages shown in the figure represent the percent variance explained by each axis, which is calculated by PC's eigenvalues divided by the sum of eigenvalues of all PCs. PC1 explains 81.2% of the variance in shape, and PC2 explains about 5.52% of the variance, which are chosen as axes of the morphospace.

3.4 Model Fitting Comparison

3.4.1 Summary Statistic of Morphological Traits

I evaluated the summary statistic of three PCs and Leaf Area, as shown in Fig. 6. As we can see, PC1 has a relatively higher mean and variance compare to the other two PCs. The medians of each PCs value are similar to the means of each PCs. The mean of leaf area is much higher than the median of leaf area, which means there more small leaves compare to large leaves.

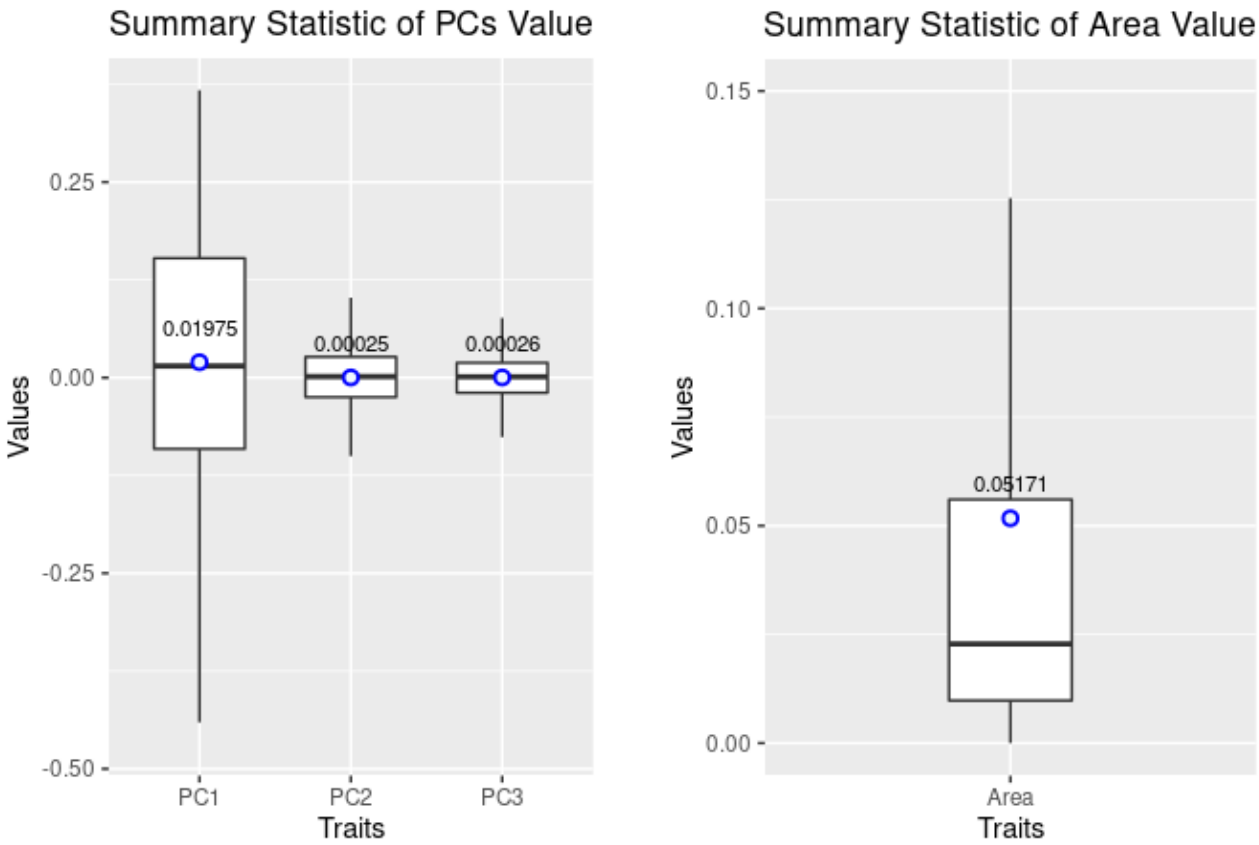

Fig. 6 Box plots of first three PCs and leaf area. The box plots show the minimum, first quartile, median, third quartile, and maximum of traits value. The blue circles and the numbers above these circles in plots represent the mean of the corresponding traits value.

3.4.2 Model Fitting on First Three PCs of Harmonic Coefficients

I first fitted the Brownian Motion Model to the first 3 PCs and the GBMB phylogeny. The BM model I used is a unique rate model, which means that the resultant rate matrix is unique for the whole phylogenetic tree. The resultant evolution rate matrix is shown in Table 1. For the summary results for the model, the AIC of the model fitting is -1402.70. From the matrices in Table 1, we can see that the variance of PC1 is higher than the variance of PC2, and the variance of PC2 is higher than the variance of PC3 in the BM model. The correlation between PC1 and PC2 and the correlation between PC2 and PC3 are similar, and the correlation between PC1 and PC3 is negative and its absolute value is very small in the BM model.

Rate Matrix (σ, BM)	PC1	PC2	PC3
PC1	0.0094	0.0022	-0.0001
PC2	0.0022	0.0024	0.0009
PC3	-0.0001	0.0009	0.0016

(a)

Corr Matrix (σ, BM)	PC1	PC2	PC3
PC1	1.0000	0.4632	-0.0258
PC2	0.4632	1.0000	0.4593
PC3	-0.0258	0.4593	1.0000

(b)

Table 1 (a) Estimated rate matrix of the Brownian Motion model on first 3 PCs (b) correlation matrix of the Brownian Motion model on first 3 PCs

I also fitted the OU model with a unique adaptive optimum per trait to the first 3 PCs, which means the optimums are unique for each trait. The resultant evolution rate matrices and the correlation matrices of optimum pulling force and random walk are shown in Table 2. For the summary results for the model, the AIC of model fitting is -8583.22. From the matrices, we can see that, in the OU model, PC1 shows a much higher σ value than the other PCs, indicating that the Brownian Motion has a powerful effect on PC1, suggesting that the evolution of PC1 is more like a random process compare to other two PCs. On the other hand, the PC2 and PC3 show a relatively higher α value than the PC1, meaning these two PCs have a strong pull towards optimums.

Rate Matrix (α, OU)	PC1	PC2	PC3
PC1	9.2596	10.6893	0.7756
PC2	10.6893	85.1588	61.3903
PC3	0.7756	61.3903	98.5915

(a)

Rate Matrix (σ, OU)	PC1	PC2	PC3
PC1	0.4419	0.2565	0.0147
PC2	0.2565	0.2790	0.1813
PC3	0.0147	0.1813	0.2296

(b)

Corr Matrix (α, OU)	PC1	PC2	PC3
PC1	1.0000	0.3807	0.0135
PC2	0.3807	1.0000	0.0606
PC3	0.0257	0.6700	1.0000

(c)

Corr Matrix (σ, OU)	PC1	PC2	PC3
PC1	1.0000	0.7305	0.0461
PC2	0.7305	1.0000	0.7163
PC3	0.0461	0.7163	1.0000

(d)

Table 2 Fitting result of the Ornstein Uhlenbeck model on first 3 PCs (a) Estimated rate matrix of α, which represents the strength of pulling force (b) Estimated rate matrix of σ, which represents the strength of random walk (c) Correlation matrix of α (d) Correlation matrix of σ

I compared the summary results of two models. From the result, the fitting of the OU model has a relatively smaller AIC than the fitting of the BM model, which suggests that the OU model fits better to leaf shape and the phylogeny than the BM model. This implies that the leaf shape evolution has a pulling force towards optimum.

3.4.3 Model Fitting on Leaf Area

I fitted the BM Model to the leaf area and the phylogeny. The resultant evolution rate of the leaf area is 0.0025, and the AIC of the model fitting is -525.00. I also fitted the OU Model to leaf area and the phylogeny. The resultant strength of the pulling force (α) of the leaf area evolution is 5.6041, the strength of random walks of the leaf area evolution (σ) is 0.0935, and the AIC of the model fitting is -1987.88. From the result, the fitting of the OU model has a smaller AIC than the fitting of the BM model, which suggests that the OU model fits better to leaf area and the phylogeny than the BM model. This implies that the evolution of leaf area also has a pulling force towards optimum.

4 Discussion

4.1 PointRend Mask R-CNN

Digitized herbarium specimen has several kinds of noise objects in their background, increasing the difficulty of extracting leaf. PointRend shows a good separation between leaf and noise objects. In most cases, only objects with similar color and shapes to leaves, such as conifer cones and pods (which sometimes have similar shapes to leaves in images), are sometimes mislabeled. The edge of masks fits instances well, which is better than the Mask R-CNN method.

I found a problem that PointRend Mask R-CNN sometimes covers some pixels of other leaves segments into the masks if leaves stick together, as shown in Fig. 7. This problem occurs more with the PointRend method due to its unique point-wise labeling methods, which sometimes cause the labeling of points to focus only on a small area. However, PointRend Mask R-CNN still covers more details than the classic Mask R-CNN methods, and it is more suitable for extracting target objects for further morphometric analysis. In this case, besides the segment of leaves, PointRend Mask R-CNN can also extract other leaf organs and organs from other organisms, such as insects, birds, and mammals.

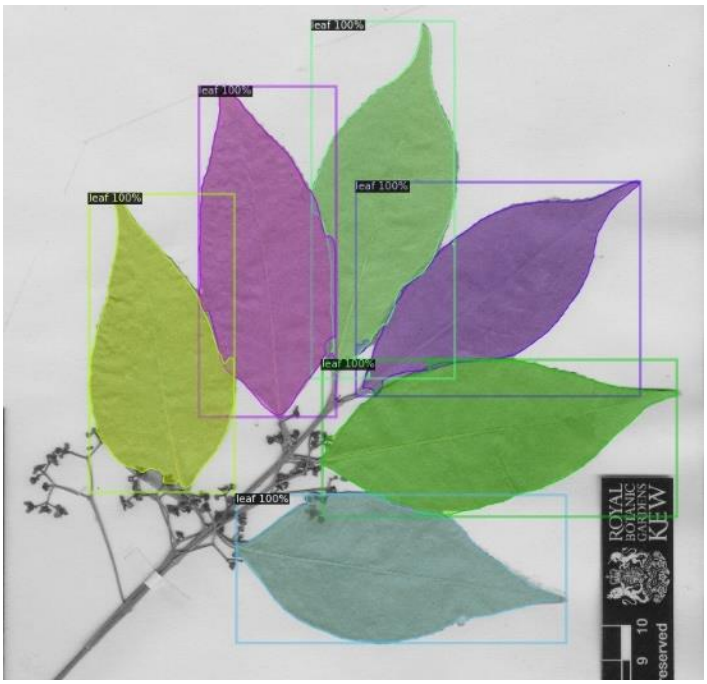

Fig. 7 An example of masks cover parts of other leaves masks. When the masks are close to each other on the specimen image, masks generated by PointRend Mask R-CNN will sometime cover parts of other leaf masks and become less accurate.

4.2 Filtering of the Leaf Masks

The RF model filters out many masks, which is actually good as many masks generated from herbarium specimens are fragments of leaves. Although the rest of the masks still contains some leaf fragment masks, it still provides a better result than either just passing the masks to morphological trait extraction. As the filtering process only takes binarized mask images, information is lost when judging the mask, such as color, texture, and local environments that help make decisions. In this case, to improve the result of the filtering by the RF model, these kinds of features and information should also be included in the analysis. When extracting the mask, a supplement description of leaf color can also be included to make a better inference, which is also an important trait of leaves.

4.3 Extracting the Leaf Shape with EFA

From the result of EFA and PCA, PC1 explains most part of the variance, which shows that the evolution of the leaf's shapes is mainly based on the variance of PC1. From the morphospace of PC1 and PC2 (Fig. 5), we can see that one end of PC1 shows a relatively round leaf and another shows a thin leaf, which implies that the variances of the leaf shape in evolution are based on this change of leaf roundness. For PC2 in the morphospace, it describes the skewness of the leaf, and the shapes on two ends are mirror images of the shapes on the other end. This kind of skewness is also crucial for determining the shape of leaves, as some leaves are more skew to the petiole of the leaves, and others are more skew to the tips (Nicotra *et al*., (2011)). The previous study shows that this kind of skewness also influences the functional leaf size (Jones *et al*., (2009); Shi *et al*., (2019)). However, one problem is that this is actually hard for the EFA to determine which end of the leaves mask is connected to the stem of the plant, as this information is lost after segmentation. To solve this problem, one potential solution is to extract the relative position of the stem and other leaves, which can help determine which end of the leaves are more likely to connect to the stem.

4.4 PCM Model Fitting

The PCs fit well to the BM and OU models. OU model shows a better fitting to the PCs, indicating that the evolution of these PCs shows a pulling force towards optimums. This phenomenon has been mentioned in past research (Uyeda *et al*., (2015)), as the first few PCs axes always show regular pattern support for the OU model, while the last few PCs have equivocal support for either a BM or OU model if the trait variables are evolved in a correlated or uncorrelated OU process. However, as the evolution of leaf area also shows pulling forces towards optimum, we can still say that the evolution of leaf morphological trait favors OU model and have pulling force towards optimums.

The variances of α in the OU rate matrix are always high compared to the variance of σ, which shows that the strength of pull is high when the difference between the current trait and optimum is large. When the difference becomes smaller, the pulling force will become smaller, and the modes of leaf evolution gradually become random walks.

From the correlation matrices in Tables (1) and (2), the correlation between PC1 and PC2 and the correlation between PC2 and PC3 are large when comparing their covariance to the variance. This may imply that the components of shape evolve jointly, which has also been mentioned in previous studies (Jones *et al*., (2009)). The correlations between shape components may cause by genetic constraints, ontogenetic integration, or correlated selection of plants (Caetano, & Harmon, (2017)).

Although the max-min normalization affects the variance and the mean of area, it doesn't affect the comparison of model fitting and the analysis of evolutionary patterns of leaf area, as the values of area are

affected by constants. The model fitting to leaf area and the phylogeny also shows that the OU model favors more than the BM model. This implies that there is a potential pulling force toward optimums. The stabilizing selection happens in the evolution of leaf size, which means that the size of the leaf influences the performance of leaf function. This is true as several important physiological traits, such as leaf mass per area, are correlated to the size of leaves (Givnish T. J. & Vermeij G. J., (1976)).

4.5 Further Research

I annotated the training dataset for the segmentation network with VIA, which is a manually labeling tool. Recent studies about object detection have pointed out that it is possible to label the image with AI assistance (Weeks *et al*., (2022)). Tools like Toronto Annotation Suite can accelerate the annotation process, which is helpful when annotating a large dataset and can help solve the potential problem of overfitting the training datasets (Amlan *et al*., (2021)).

When filtering the damaged leaves, it is also possible to repair the damaged leaves with a recognizable outer shape with image processing methods. Methods like flood-fill operation can be applied to the leaves with holes inside, providing more valid masks for further analysis (Meineke *et al*., (2019); Hussein *et al*., (2021)).

Recently, some studies suggests that it will be more beneficial to use semantic segmentation instead of instance segmentation for extracting a single leaf from the herbarium specimen (Hussein et al. (2021)). This method identifies leaves overlapped on the image as a single entity. The semantic segmentation method may filter out much more leaf masks than the instance segmentation method. However, the resultant leaf masks are guaranteed to be single leaves without overlapping, which have better quality. When filtering the result, besides using the RF methods, a supporting vector machine (SVM) can be trained to classify the mask outputs. SVM is designed for classification based on continuous data, which is suitable for this project (Hussein *et al*., (2021)).

5 Conclusions

In summary, this project shows that it is possible to study the leaf trait evolution by using a deep learning network to extract leaf masks from digitized herbarium specimens. Morphological traits can be extracted from the leaf masks to study leaf evolution patterns with PCM. From the results of PCA on the harmonic coefficient, which are used to describe the leaf shape, PC1 explains most part of the leaf shape variance. The correlations between PCs are small, meaning that leaf shape components are evolved separately. From the result of the PCM model fitting, the OU model fits better than the BM model to both harmonic coefficients PCs and leaf area, which implies that the mode of evolution is the random walks with pulling forces towards the optimum, and stabilized selection may happens in the evolution of leaves.

Acknowledgement

I would like to express my deepest appreciation to my main supervisor Dr. Will Pearse for his patient guidance, correction of my mistakes, and encouragement throughout this project under such a pandemic situation. Many thanks to my supervisors Dr. Gemma Bramley and Dr. Alexander Zuntini, for teaching me how to download images from the GBIF website. I also would like to express my appreciation to Mahika Dixit for her patient guidance in giving useful advices on the dissertation draft. I want to express my appreciation to my friends Jiaze Li and Yuming Shi for sharing their knowledge on evolution and advice on my project. I want to express my appreciation to my family and friends that encourage me and smooth my sorrow during this whole year under such as pandemic situation.

Data and Code Availability

The input herbarium specimen images downloaded from the GBIF's website are available through the following link:
https://drive.google.com/drive/folders/1y_YDAjG4WPllf2m6Xf8qCD11Ybg9Spdo?usp=sharing
The output images and masks generated from classic Mask R-CNN and PointRend Mask R-CNN are available through the following link:
https://drive.google.com/drive/folders/1Ey-kkdUS5eFVHWYIzkIWKrCzMl5OdO-v?usp=sharing
The training and testing datasets for training classic Mask R-CNN and PointRend Mask R-CNN are available through the following link:
https://drive.google.com/drive/folders/16ORv4jLcdUSFUFr6V0pygdB9BJZD6kPO?usp=sharing
The codes of classic Mask R-CNN and PointRend Mask R-CNN are available through the following link:
https://drive.google.com/drive/folders/1Tpv0L-FwYFYP3goZoZvlrlKOdL0RtVsp?usp=sharing
The models of classic Mask R-CNN and PointRend Mask R-CNN are available through the following link:
https://drive.google.com/drive/folders/1B3uNXgOZ3x1u_38sEpB9iPYAK2zIkqJH?usp=sharing
The training and testing datasets for training RF models are available through the following link:
https://drive.google.com/file/d/1x_wmfLjTOkUV2hDmBErkFLf5Ct9lpofx/view?usp=sharing
The R pipeline of EFA, PCA and mvMORPH for traits extraction, filtering and model fitting are available through the following link:
https://drive.google.com/file/d/18LWEi7Tf5vyYS2Wz8swTdA-CB_hCt8o4/view?usp=sharing

Reference

1. Poorter, L., & Bongers, F. (2006). Leaf traits are good predictors of plant performance across 53 rain forest species. Ecology, 87(7), 1733-1743.
2. Lusk, C. H. (2002). Leaf area accumulation helps juvenile evergreen trees tolerate shade in a temperate rainforest. Oecologia, 132(2), 188-196.
3. Reich, P. B., Ellsworth, D. S., Walters, M. B., Vose, J. M., Gresham, C., Volin, J. C., & Bowman, W. D. (1999). Generality of leaf trait relationships: a test across six biomes. Ecology, 80(6), 1955-1969.
4. Kröber, W., Plath, I., Heklau, H., & Bruelheide, H. (2015). Relating stomatal conductance to leaf functional traits. JoVE (Journal of Visualized Experiments), (104), e52738.
5. Easlon, H. M., & Bloom, A. J. (2014). Easy Leaf Area: Automated digital image analysis for rapid and accurate measurement of leaf area. Applications in plant sciences, 2(7), 1400033.
6. Shi, P., Liu, M., Ratkowsky, D. A., Gielis, J., Su, J., Yu, X., ... & Schrader, J. (2019). Leaf area–length allometry and its implications in leaf shape evolution. Trees, 33(4), 1073-1085.
7. Dornbusch, T., Watt, J., Baccar, R., Fournier, C., & Andrieu, B. (2011). A comparative analysis of leaf shape of wheat, barley and maize using an empirical shape model. Annals of botany, 107(5), 865-873.
8. Piazza, P., Jasinski, S., & Tsiantis, M. (2005). Evolution of leaf developmental mechanisms. New Phytologist, 167(3), 693-710.
9. Jones, C. S., Bakker, F. T., Schlichting, C. D., & Nicotra, A. B. (2009). Leaf shape evolution in the south African genus Pelargonium l'Her.(Geraniaceae). Evolution: International Journal of Organic Evolution, 63(2), 479-497.
10. Givnish, T. J., & Vermeij, G. J. (1976). Sizes and shapes of liane leaves. The American Naturalist, 110(975), 743-778.
11. Slater, G. J., Harmon, L. J., & Alfaro, M. E. (2012). Integrating fossils with molecular phylogenies improves inference of trait evolution. Evolution: International Journal of Organic Evolution, 66(12), 3931-3944.
12. Reich, P. B., Walters, M. B., & Ellsworth, D. S. (1997). From tropics to tundra: global convergence in plant functioning. Proceedings of the National Academy of Sciences, 94(25), 13730-13734.
13. Adler, P. B., Salguero-Gómez, R., Compagnoni, A., Hsu, J. S., Ray-Mukherjee, J., Mbeau-Ache, C., & Franco, M. (2014). Functional traits explain variation in plant life history strategies. Proceedings of the National Academy of Sciences, 111(2), 740-745.
14. Lavorel, S., & Garnier, É. (2002). Predicting changes in community composition and ecosystem functioning from plant traits: revisiting the Holy Grail. Functional ecology, 16(5), 545-556.
15. Bruelheide, H., Dengler, J., Purschke, O., Lenoir, J., Jiménez-Alfaro, B., Hennekens, S. M., ... & Jandt, U. (2018). Global trait–environment relationships of plant communities. Nature ecology & evolution, 2(12), 1906-1917.

16. Figueirido, B., Serrano-Alarcón, F. J., Slater, G. J., & Palmqvist, P. (2010). Shape at the cross-roads: homoplasy and history in the evolution of the carnivoran skull towards herbivory. Journal of Evolutionary Biology, 23(12), 2579-2594.
17. Cornwell, W., & Nakagawa, S. (2017). Phylogenetic comparative methods. Current Biology, 27(9), R333-R336.
18. Weeks, B. C., Zhou, Z., O'Brien, B. K., Darling, R., Dean, M., Dias, T., ... & Fouhey, D. F. (2022). A deep neural network for high-throughput measurement of functional traits on museum skeletal specimens. Methods in Ecology and Evolution.
19. Smith, S. A., & Brown, J. W. (2018). Constructing a broadly inclusive seed plant phylogeny. American journal of botany, 105(3), 302-314.
20. Cooper, N., Thomas, G. H., Venditti, C., Meade, A., & Freckleton, R. P. (2016). A cautionary note on the use of Ornstein Uhlenbeck models in macroevolutionary studies. Biological Journal of the Linnean Society, 118(1), 64-77.
21. Caetano, D. S., & Harmon, L. J. (2017). ratematrix: an R package for studying evolutionary integration among several traits on phylogenetic trees. Methods in Ecology and Evolution, 8(12), 1920-1927.
22. Hussein, B. R., Malik, O. A., Ong, W. H., & Slik, J. W. F. (2021). Automated extraction of phenotypic leaf traits of individual intact herbarium leaves from herbarium specimen images using deep learning based semantic segmentation. Sensors, 21(13), 4549.
23. Uyeda, J. C., Caetano, D. S., & Pennell, M. W. (2015). Comparative analysis of principal components can be misleading. Systematic Biology, 64(4), 677-689.
24. Revell, L. J., & Harmon, L. J. (2008). Testing quantitative genetic hypotheses about the evolutionary rate matrix for continuous characters. Evolutionary Ecology Research, 10(3), 311-331.
25. Triki, A., Bouaziz, B., Gaikwad, J., & Mahdi, W. (2021). Deep leaf: Mask R-CNN based leaf detection and segmentation from digitized herbarium specimen images. Pattern Recognition Letters, 150, 76-83.
26. He, K., Gkioxari, G., Dollár, P., & Girshick, R. (2017). Mask r-cnn. In Proceedings of the IEEE international conference on computer vision (pp. 2961-2969).
27. Kirillov, A., Wu, Y., He, K., & Girshick, R. (2020). Pointrend: Image segmentation as rendering. In Proceedings of the IEEE/CVF conference on computer vision and pattern recognition (pp. 9799-9808).
28. Schrader, J., Shi, P., Royer, D. L., Peppe, D. J., Gallagher, R. V., Li, Y., ... & Wright, I. J. (2021). Leaf size estimation based on leaf length, width and shape. Annals of Botany, 128(4), 395-406.
29. Liu, X., Zhao, D., Jia, W., Ji, W., Ruan, C., & Sun, Y. (2019). Cucumber fruits detection in greenhouses based on instance segmentation. IEEE Access, 7, 139635-139642.
30. Katabuchi, M. (2015). LeafArea: an R package for rapid digital image analysis of leaf area. Ecological Research, 30(6), 1073-1077.

31. Caple, J., Byrd, J., & Stephan, C. N. (2017). Elliptical Fourier analysis: fundamentals, applications, and value for forensic anthropology. International Journal of Legal Medicine, 131(6), 1675-1690.
32. Schmittbuhl, M., Le Minor, J. M., Schaaf, A., & Mangin, P. (2002). The human mandible in lateral view: elliptical Fourier descriptors of the outline and their morphological analysis. Annals of Anatomy-Anatomischer Anzeiger, 184(2), 199-207.
33. Kuhl, F. P., & Giardina, C. R. (1982). Elliptic Fourier features of a closed contour. Computer graphics and image processing, 18(3), 236-258.
34. Adams, D. C., & Otárola-Castillo, E. (2013). geomorph: an R package for the collection and analysis of geometric morphometric shape data. Methods in ecology and evolution, 4(4), 393-399.
35. Bonhomme, V., Picq, S., Gaucherel, C., & Claude, J. (2014). Momocs: outline analysis using R. Journal of Statistical Software, 56(13), 24-p.
36. Blomberg, S. P., & Garland Jr, T. (2002). Tempo and mode in evolution: phylogenetic inertia, adaptation and comparative methods. Journal of Evolutionary Biology, 15(6), 899-910.
37. Cooper, N., & Purvis, A. (2010). Body size evolution in mammals: complexity in tempo and mode. The American Naturalist, 175(6), 727-738.
38. Hunt, G. (2012). Measuring rates of phenotypic evolution and the inseparability of tempo and mode measuring rates of phenotypic evolution. Paleobiology, 38(3), 351-373.
39. Gupta, S., Rosenthal, D. M., Stinchcombe, J. R., & Baucom, R. S. (2020). The remarkable morphological diversity of leaf shape in sweet potato (Ipomoea batatas): The influence of genetics, environment, and G× E. New Phytologist, 225(5), 2183-2195.
40. Clavel, J., Escarguel, G., & Merceron, G. (2015). mvMORPH: an R package for fitting multivariate evolutionary models to morphometric data. Methods in Ecology and Evolution, 6(11), 1311-1319.
41. Nicotra, A. B., Leigh, A., Boyce, C. K., Jones, C. S., Niklas, K. J., Royer, D. L., & Tsukaya, H. (2011). The evolution and functional significance of leaf shape in the angiosperms. Functional Plant Biology, 38(7), 535-552.
42. Speiser, J. L., Miller, M. E., Tooze, J., & Ip, E. (2019). A comparison of random forest variable selection methods for classification prediction modeling. Expert systems with applications, 134, 93-101.
43. Reich, P. B., Wright, I. J., Cavender-Bares, J., Craine, J. M., Oleksyn, J., Westoby, M., & Walters, M. B. (2003). The evolution of plant functional variation: traits, spectra, and strategies. International Journal of Plant Sciences, 164(S3), S143-S164.
44. He, K., Zhang, X., Ren, S., & Sun, J. (2016). Deep residual learning for image recognition. In Proceedings of the IEEE conference on computer vision and pattern recognition (pp. 770-778).
45. Pan, S. J., & Yang, Q. (2009). A survey on transfer learning. IEEE Transactions on knowledge and data engineering, 22(10), 1345-1359.

46. Harmon, L. J., Losos, J. B., Jonathan Davies, T., Gillespie, R. G., Gittleman, J. L., Bryan Jennings, W., ... & Mooers, A. Ø. (2010). Early bursts of body size and shape evolution are rare in comparative data. Evolution: International Journal of Organic Evolution, 64(8), 2385-2396.
47. Klingenberg, C. P., & Marugán-Lobón, J. (2013). Evolutionary covariation in geometric morphometric data: analyzing integration, modularity, and allometry in a phylogenetic context. Systematic biology, 62(4), 591-610.
48. Breiman, L. (2001). Random forests. Machine learning, 45(1), 5-32.
49. Amlan Kar, Seung Wook Kim, Marko Boben, Jun Gao, Tianxing Li, Huan Ling, Zian Wang, and Sanja Fidler. (2021). Toronto annotation suite. https://aidemos.cs. toronto.edu/toras
50. Meineke, E. K., Classen, A. T., Sanders, N. J., & Jonathan Davies, T. (2019). Herbarium specimens reveal increasing herbivory over the past century. Journal of Ecology, 107(1), 105-117.
51. Rahman, M. S., & Islam, M. R. (2013, February). Counting objects in an image by marker controlled watershed segmentation and thresholding. In 2013 3rd IEEE International Advance Computing Conference (IACC) (pp. 1251-1256). IEEE.
52. Lin, T. Y., Dollár, P., Girshick, R., He, K., Hariharan, B., & Belongie, S. (2017). Feature pyramid networks for object detection. In Proceedings of the IEEE conference on computer vision and pattern recognition (pp. 2117-2125).

Supplementary SI

SI 1 Mask R-CNN Structure

Mask R-CNN is a method based on Region-Based Convolutional Neural Networks (R-CNN), which are designed to do object detection by generating region proposals (pixels that have similar patterns) from the input image, then extracting the feature of each region proposal and classifying the regions based on the features, and generates bounding box to locate the object (He *et al*., (2017)). Based on that, Mask R-CNN also labels each pixel with the class and specific object it belongs to, differentiating each instance. Mask R-CNN contains two stages: the first stage is the Region Proposal Network (RPN), which proposes candidate objects with bounding boxes based on a regular grid; the second stage generates binary masks for each ROI and classes independently, which is in parallel to predicting classes and bounding boxes.

SI 2 PointRend Module Structure

A PointRend head module is added to the backbone, which accepts several feature maps generate from backbones and outputs predictions for the class labels in a grid with higher resolution. The module of PointRend consists of a point selection strategy, a point-wise feature representation, and a point-wise head prediction network (Kirillov *et al*., (2020)), as shown in Fig. 3. The network will generate a coarse prediction at the beginning. After that, the point selection strategy only selects a small number of grid points, which are ambiguous in labeling their classes based on their feature. Then, the point-wise feature representation extracted additional features for these points using several nearest neighbors of the point that are on the regular grid, and the results are passed to the point head. The point head is a small neural network used to predict a label for each independent ambiguous point based on the feature representation. After repeating several times of this point-wise prediction module, a finer mask with higher resolution will be generated.

SI 3 EFA Algorithms

The basic idea of EFA is to decompose a periodic function into a sum of simple trigonometric functions such as sine and cosine (Caple *et al*., (2017)). As leaf shapes are consisted by a closed outline, if starting from one point on the outline and follow it, it will eventually return back to the starting point, and thus, it is possible to use periodic functions to describe the outline of any closed shape (Kuhl & Giardina, (1982)). Since using the sum of a sine curve and a cosine curve can describe an ellipse, the first harmonic uses this combination to describe the outline of a leaf with an ellipse that is the best possible fit by least-squares. The first harmonic traverses the ellipse only one time in each period. When the number of harmonics is higher, the n^{th} harmonic still uses the combination of one sine curve and one cosine curve to describe an ellipse, but it traverses the ellipse nth time in each period. Finally, all harmonics are weighted and added together to describe the outline. With higher number of harmonics, the description of shapes can be more precise.

To perform EFA, the outline of the leaf mask is described with several trigonometric functions in a Cartesian coordinates system. The equation expression of outline can be expressed as:

$$\omega = \frac{2\pi}{T} \quad (1)$$

$$x(t) = \frac{a_0}{2} + \sum_{n=1}^{+\infty} a_n cos(n\omega t) + b_n sin(n\omega t) \quad (2)$$

$$y(t) = \frac{c_0}{2} + \sum_{n=1}^{+\infty} c_n cos(n\omega t) + d_n sin(n\omega t) \quad (3)$$

In equation (1) – (3), T is the perimeter of a given closed outline, which represents the period of the signal, and ω represents the pulse. The curvilinear abscissa t varies from 0 to T. $x(t)$ and $y(t)$ represent the coordinate of points on x and y axis.

Before the harmonic coefficients are calculated, it is necessary to calculate their estimators first. The estimators for every harmonic coefficient of the nth rank can be calculated by equation (4) – (7):

$$a_n = \frac{2}{T} + \int_0^T x(t) cos(n\omega t) dt \quad (4) \quad b_n = \frac{2}{T} + \int_0^T x(t) sin(n\omega t) dt \quad (5)$$

$$c_n = \frac{2}{T} + \int_0^T y(t) cos(n\omega t) dt \quad (6) \quad d_n = \frac{2}{T} + \int_0^T y(t) sin(n\omega t) dt \quad (7)$$

After the harmonic sum of trigonometric functions weighted with harmonic coefficients has been calculated, they are normalized to remove translational or rotational differences between shapes. It is done by adjusting the first harmonic, which describes the overall shape of one ellipse, and then shapes are aligned based on their first ellipse.

For each harmonic, four harmonic coefficients (A_n, B_n, C_n, D_n) per harmonic can be described. With these four harmonic coefficients for each harmonic, it is possible to express a shape that describes the outline of a mask, as shown in Fig. 4. The four harmonic coefficients can be calculated by the equation (8) – (13):

$$\begin{pmatrix} A_n & B_n \\ C_n & D_n \end{pmatrix} = \frac{1}{\lambda} \begin{pmatrix} cos\psi & sin\psi \\ -sin\psi & cos\psi \end{pmatrix} \begin{pmatrix} a_n & b_n \\ c_n & d_n \end{pmatrix} \begin{pmatrix} cosn\theta & sinn\theta \\ -sinn\theta & cosn\theta \end{pmatrix} \quad (8)$$

Where:

$$\lambda = \sqrt{a^2 + c^2}(9)\theta = arcta\, n(c^2/a^2) \quad (10)$$

$$a^2 = a_1 cos\psi + b_1 sin\psi \quad (11) \quad c^2 = c_1 cos\psi + d_1 sin\psi \quad (12)$$

$$\psi = 0.5 arctan \frac{2(a_1 b_1 + c_1 d_1)}{a_1^2 + c_1^2 - b_1^2 - d_1^2} \quad (13)$$

In this case, λ describes the magnitude of the width (semi-major axis) of the ellipse as defined by the first harmonic in equation (9), θ describes the rotation angle from the starting point to the end of the ellipse in equation (10), and ψ describes the rotation angle of the first ellipse in equation (13)